





LETTER

Intermittent, reflection-driven, strong imbalanced MHD turbulence

B.D.G. Chandran¹ , N. Sioulas², S. Bale², T. Bowen², V. David¹ ,
R. Meyrand¹  and E. Yerger¹ 

¹Space Science Center and Department of Physics and Astronomy, University of New Hampshire,
Durham, NH 03824, USA

²Space Sciences Laboratory and Department of Physics, University of California, Berkeley, CA
94720, USA

Corresponding author: B.D.G. Chandran, benjamin.chandran@unh.edu

(Received 12 August 2024; revision received 6 February 2025; accepted 18 February 2025)

We develop a phenomenological model of strong imbalanced magnetohydrodynamic (MHD) turbulence that accounts for intermittency and the reflection of Alfvén waves by spatial variations in the Alfvén speed. Our model predicts the slopes of the inertial-range Elsasser power spectra, the scaling exponents of the higher-order Elsasser structure functions and the way in which the parallel (to the magnetic field) length scale of the fluctuations varies with the perpendicular length scale. These predictions agree reasonably well with measurements of solar-wind turbulence from the Parker Solar Probe (PSP). In contrast to previous models of intermittency in balanced MHD turbulence, we find that intermittency in reflection-driven MHD turbulence increases the parallel wavenumbers of the energetically dominant fluctuations at small perpendicular length scales. This, like the PSP measurements with which our model agrees, suggests that turbulence in the solar wind and solar corona may lead to more ion cyclotron heating than previously realized.

Keywords: Astrophysical plasmas, space plasma physics, plasma nonlinear phenomena

1. Introduction

Magnetohydrodynamic (MHD) turbulence has been an active area of research for over sixty years. Part of the interest in MHD turbulence stems from its importance as a model for plasma turbulence in the solar corona, solar wind and more distant astrophysical settings. In this paper, we focus on non-compressive, Alfvénic fluctuations, for which the energy density of the magnetic-field fluctuations and velocity fluctuations are comparable. Such fluctuations are the dominant component of solar-wind turbulence (Tu & Marsch 1995).

Non-compressive, Alfvénic turbulence is conventionally studied using one of three approximate forms of the MHD equations: incompressible MHD (Elsasser 1950); reduced MHD (Kadomtsev & Pogutse 1974; Strauss 1976; Schekochihin *et al.* 2009); and a generalization of the reduced MHD equations that accounts for a radially stratified and expanding background plasma (see, e.g. Dmitruk & Matthaeus 2003; Perez & Chandran 2013; van Ballegooijen *et al.* 2011; van Ballegooijen & Asgari-Targhi 2016, 2017). All three approximations are usefully expressed in terms of the Elsasser variables (Elsasser 1950),

$$\mathbf{z}^{\pm} = \mathbf{v} \pm \frac{\mathbf{B}}{(4\pi\rho)^{1/2}}, \quad (1.1)$$

where \mathbf{v} , \mathbf{B} and ρ are the velocity, magnetic field and mass density, respectively. In the presence of a mean magnetic field \mathbf{B}_0 , and when the fluctuations in \mathbf{z}^{\pm} are small compared with the Alfvén velocity $v_A = \mathbf{B}/\sqrt{4\pi\rho}$, the \mathbf{z}^{\pm} fluctuations are Alfvén waves that propagate at velocity $\mp v_A$. In Alfvénic turbulence in homogeneous plasmas, only counter-propagating fluctuations interact nonlinearly (Kraichnan 1965). In addition, small-scale Alfvénic fluctuations with correlation length λ propagate along the local background magnetic field obtained by summing \mathbf{B}_0 and the magnetic field associated with all fluctuations with correlation lengths $\gg \lambda$ (Kraichnan 1965). In contrast to hydrodynamic turbulence, Alfvénic turbulence is intrinsically anisotropic (Montgomery & Turner 1981), both in the weak-turbulence regime (Shebalin, Matthaeus & Montgomery 1983; Ng & Bhattacharjee 1996, 1997; Galtier *et al.* 2000) and strong-turbulence regime (Goldreich & Sridhar 1995; Cho & Vishniac 2000). In particular, as energy cascades from large scales to small scales, the small-scale structures that are produced are elongated along \mathbf{B} .

Three frontiers in the study of MHD turbulence are imbalance, intermittency and inhomogeneity. In imbalanced turbulence, the fluctuations in one of the Elsasser variables are much larger than the fluctuations in the other Elsasser variable (see, e.g. Lithwick, Goldreich & Sridhar 2007; Beresnyak & Lazarian 2008; Chandran 2008; Perez & Boldyrev 2009; Podesta & Bhattacharjee 2010; Schekochihin 2022). Intermittency refers to the phenomenon in which the majority of the fluctuation energy at scale λ is concentrated into a fraction of the volume that decreases as λ decreases (see, e.g. Frisch 1996). Inhomogeneity, and in particular the variation of v_A with heliocentric distance r , results in the reflection of Alfvén waves (Heinemann & Olbert 1980; Velli 1993; Hollweg & Isenberg 2007; Verdini & Velli 2007). The Sun launches only outward-propagating Alfvén waves into coronal holes¹ and the solar wind, and inhomogeneity leads to the mix of \mathbf{z}^+ and \mathbf{z}^- fluctuations that is needed in order for the fluctuations to interact (Velli, Grappin & Mangeney 1989; Matthaeus *et al.* 1999; Meyrand *et al.* 2025).

In this paper, we develop a model of Alfvénic turbulence that accounts for all three of these phenomena. We note that intermittency, which in some ways is the most complicated of the three, has two relatively simple consequences. First, because \mathbf{z}^+ fluctuations interact only with \mathbf{z}^- fluctuations and *vice versa*, and because the energetically dominant \mathbf{z}^+ and \mathbf{z}^- fluctuations are confined to largely distinct fractions of the volume, intermittency makes it harder for a strong \mathbf{z}^+ fluctuation to ‘find’ a strong \mathbf{z}^- fluctuation with which to interact. Moreover, since the volume filling factor f_{λ} of the energetically dominant \mathbf{z}^{\pm} fluctuations decreases as

¹Coronal holes are regions of the solar corona threaded by ‘open magnetic-field lines’, which connect the solar surface to the distant solar wind.

λ decreases, intermittency decelerates the cascade to an increasing degree as λ decreases, thereby flattening the inertial-range power spectrum relative to models in which intermittency is neglected (Maron & Goldreich 2001).² Second, because f_λ decreases as λ decreases, near the dissipation scale the fluctuations that dominate the energy have much larger amplitudes than the root-mean-square fluctuation amplitude computed over the entire volume, which can enhance the efficiency of certain heating mechanisms such as stochastic ion heating (see, e.g. Mallet *et al.* 2019).

2. The inertial range of reflection-driven Alfvénic turbulence

We view Alfvénic turbulence as a collection of localized, non-compressive fluctuations in the Elsasser variables \mathbf{z}^\pm defined in (1.1) and take these fluctuations to be characterized by length scales λ and l_λ^\pm perpendicular and parallel to the magnetic field, respectively. We define the Elsasser increment

$$\Delta \mathbf{z}_\lambda^\pm(\mathbf{x}, \hat{\mathbf{s}}, t) = \mathbf{z}^\pm(\mathbf{x} + 0.5\lambda\hat{\mathbf{s}}, t) - \mathbf{z}^\pm(\mathbf{x} - 0.5\lambda\hat{\mathbf{s}}, t), \quad (2.1)$$

where $\hat{\mathbf{s}}$ is a unit vector perpendicular to \mathbf{B} , and we take

$$\delta z_\lambda^\pm(\mathbf{x}, t) = \frac{1}{2\pi} \int_0^{2\pi} d\theta |\Delta \mathbf{z}_\lambda^\pm(\mathbf{x}, \hat{\mathbf{s}}, t)| \quad (2.2)$$

to be the characteristic amplitude of the \mathbf{z}^\pm structure of perpendicular scale λ at position \mathbf{x} and time t , where the angle θ specifies the direction of $\hat{\mathbf{s}}$ within the plane perpendicular to \mathbf{B} .

In intermittent turbulence, the tail of the distribution of fluctuation amplitudes becomes increasingly prominent as λ decreases. To account for this, we follow an approach that has been used in two previous studies of balanced, intermittent reduced MHD (RMHD) turbulence: Chandran, Schekochihin & Mallet (2015) and Mallet & Schekochihin (2017), which we henceforth refer to as CSM15 and MS17, respectively. In particular, we parameterize the scale-dependence of the fluctuation-amplitude distribution by treating δz_λ^\pm as a random variable given by the equation

$$\delta z_\lambda^\pm = \bar{z}^\pm \beta^q, \quad (2.3)$$

where \bar{z}^\pm is a scale-independent random number, β is a constant satisfying $0 < \beta < 1$ that we will determine in the analysis to follow, and q is a random integer that is uncorrelated with \bar{z}^\pm and that has a Poisson distribution with scale-dependent mean μ ,³

$$P(q) = \frac{e^{-\mu} \mu^q}{q!}. \quad (2.4)$$

For simplicity, we have taken μ and β to be the same for δz_λ^+ and δz_λ^- , but we assume that

$$\langle \bar{z}^+ \rangle \gg \langle \bar{z}^- \rangle, \quad (2.5)$$

as we consider imbalanced turbulence, where $\langle \dots \rangle$ denotes an ensemble average.

²In contrast, in hydrodynamic turbulence, eddies interact with themselves, so intermittency acts to accelerate the cascade to an increasing degree as the eddy size decreases, thereby steepening the inertial-range power spectrum (She & Leveque 1994).

³The PDF of $\log_\beta \delta z_\lambda^\pm$ is then the convolution of the PDF of $\log_\beta(\bar{z}^\pm)$ with the discrete Poisson distribution. If \bar{z}^\pm were replaced by a constant, then δz_λ^\pm would have a log-Poisson distribution.

Given (2.3) and (2.4), the volume filling factor of the most intense fluctuations is $P(0) = e^{-\mu}$. As in several previous studies of intermittent MHD turbulence (Grauer, Krug & Marliani 1994; Politano & Pouquet 1995; Chandran *et al.* 2015; Mallet & Schekochihin 2017), we take this filling factor to be $\propto \lambda$ and therefore set

$$\mu = A + \ln \left(\frac{L_{\perp}}{\lambda} \right), \quad (2.6)$$

where A is a constant that characterizes the breadth of the distribution of fluctuation amplitudes at the perpendicular outer scale L_{\perp} . We discuss the possible physical origins of this scaling in § 4.1.

Equation (2.6) implies that $\mu \gg 1$ within the inertial range, in which $\lambda \ll L_{\perp}$. It follows from (2.4) that both the most common value of q and the median value of q are $\simeq \mu$ (Choi 1994), and hence the most common fluctuation amplitude at scale λ and the median fluctuation amplitude at scale λ are approximately

$$w_{\lambda}^{\pm} = \langle \bar{z}^{\pm} \rangle \beta^{\mu} \propto e^{\mu \ln \beta} \propto \lambda^{-\ln \beta}. \quad (2.7)$$

Fluctuations with $q \ll \mu$ satisfy $\delta z_{\lambda}^{\pm} \gg w_{\lambda}^{\pm}$ and form the tail of the distribution, which becomes broader as λ decreases and μ increases.

The functional form of $P(q)$ makes it straightforward to compute the n th-order structure function of δz_{λ}^{\pm} ,

$$\langle (\delta z_{\lambda}^{\pm})^n \rangle = \langle (\bar{z}^{\pm})^n \rangle e^{-\mu} \sum_{q=0}^{\infty} \frac{(\mu \beta^n)^q}{q!} = \langle (\bar{z}^{\pm})^n \rangle e^{-\mu + \mu \beta^n}, \quad (2.8)$$

where we have utilized the Taylor expansion $\sum_{q=0}^{\infty} x^q / q! = e^x$. The scaling exponent ζ_n of the n th-order structure function is defined by the proportionality relation

$$\langle (\delta z_{\lambda}^{\pm})^n \rangle \propto \lambda^{\zeta_n}. \quad (2.9)$$

Upon substituting (2.6) into (2.8), we obtain (Chandran *et al.* 2015; Mallet & Schekochihin 2017)

$$\zeta_n = 1 - \beta^n. \quad (2.10)$$

As q increases from 0, the summand in (2.8) increases until q reaches a value $\simeq \mu \beta^n$, after which the summand decreases with increasing q . The amplitudes of the fluctuations that make the largest contribution to $\langle (\delta z_{\lambda}^{\pm})^n \rangle$ are thus approximately

$$\delta z_{(n),\lambda}^{\pm} = \bar{z}^{\pm} \beta^{\mu \beta^n} \propto \lambda^{-\beta^n \ln \beta}. \quad (2.11)$$

It follows from (2.7) and (2.11) that $w_{\lambda}^{\pm} = \delta z_{(0),\lambda}^{\pm} < \delta z_{(1),\lambda}^{\pm} < \delta z_{(2),\lambda}^{\pm} < \dots$. As n increases, $\mu \beta^n$ decreases, and $\delta z_{(n),\lambda}^{\pm}$ characterizes the amplitudes of fluctuations that are farther out in the tail of the distribution.

We restrict our attention to the strong-turbulence regime, in which the time $\tau_{\text{nl},\lambda}^{-} \sim \lambda / \delta z_{\lambda}^{+}$ required for a δz_{λ}^{+} fluctuation to shear a δz_{λ}^{-} fluctuation is comparable to or smaller than the time $\tau_{\text{lin},\lambda}^{-} \sim l_{\lambda}^{+} / (2v_A)$ required for a point moving with the δz_{λ}^{-}

fluctuation at velocity v_A to pass through the (counter-propagating) δz_λ^+ fluctuation. In other words, we assume that

$$\chi_\lambda^+ \equiv \frac{\delta z_\lambda^+ l_\lambda^+}{\lambda v_A} \gtrsim 1. \quad (2.12)$$

In this limit, each cross-section (in the plane perpendicular to \mathbf{B}) of a propagating δz_λ^- structure is strongly deformed after a time $\sim \lambda/\delta z_\lambda^+$, causing the parallel correlation length of the δz_λ^- fluctuation to satisfy (Lithwick *et al.* 2007)

$$l_\lambda^- \sim \frac{v_A \lambda}{\delta z_\lambda^+}. \quad (2.13)$$

Two locations within a δz_λ^+ structure separated by a distance l_λ^- along the magnetic field are deformed by δz_λ^- structures in uncorrelated ways, and hence (Lithwick *et al.* 2007)

$$l_\lambda^+ \simeq l_\lambda^-. \quad (2.14)$$

Henceforth (except in §4), we will drop the distinction between l_λ^+ and l_λ^- and use simply l_λ . Equations (2.13) and (2.14) imply that the inequality in (2.12) is replaced by the critical-balance relation

$$\chi_\lambda^+ \sim 1, \quad (2.15)$$

which states that $\tau_{\text{nl},\lambda}^- \sim \tau_{\text{lin},\lambda}^-$ at all scales (Goldreich & Sridhar 1995; Lithwick *et al.* 2007) and within structures of differing amplitudes at the same scale (Mallet, Schekochihin & Chandran 2015).

We define

$$\epsilon_\lambda^+ = \frac{(\delta z_\lambda^+)^2}{\tau_{\text{nl},\lambda}^+}, \quad (2.16)$$

which is the rate at which a localized δz_λ^+ fluctuation's energy cascades to smaller scales, where $\tau_{\text{nl},\lambda}^+$ is the energy cascade time scale of the δz_λ^+ fluctuation. In reflection-driven MHD turbulence in the solar wind, the fluctuations propagating towards the Sun in the plasma frame (the z^- fluctuations) are produced by the reflection of the outward-propagating z^+ fluctuations (Heinemann & Olbert 1980; Velli 1993; Hollweg & Isenberg 2007). The z^- fluctuations are also subsequently sheared and cascaded by nonlinear interactions with z^+ fluctuations (Velli *et al.* 1989). As a consequence, in a reference frame that propagates with the z^+ fluctuations away from the Sun, the z^- fluctuations at scale λ remain coherent until the z^+ fluctuations at scale λ evolve due to nonlinear interactions (Lithwick *et al.* (2007); see also §5 of Chandran & Perez (2019)). This ‘anomalous coherence’ implies that the z^+ fluctuations at scale λ have a cascade time scale

$$\tau_{\text{nl},\lambda}^+ \sim \frac{\lambda}{\delta z_\lambda^-}, \quad (2.17)$$

even though this time exceeds the time $\sim l_\lambda/2v_A$ required for z^+ and z^- structures at perpendicular scale λ to propagate through each other at the Alfvén speed.

For values of λ in the inertial range, we assume that the average cascade flux is independent of λ :

$$\langle \epsilon_\lambda^+ \rangle \propto \lambda^0. \quad (2.18)$$

Upon substituting (2.16) and (2.17) into (2.18), we obtain

$$\left\langle \frac{(\delta z_{\lambda}^+)^2 \delta z_{\lambda}^-}{\lambda} \right\rangle \propto \lambda^0. \quad (2.19)$$

We cannot evaluate the left-hand side of (2.19) by separately averaging $(\delta z_{\lambda}^+)^2$ and δz_{λ}^- using (2.3) and (2.4), because z^+ and z^- fluctuations interact with each other, causing δz_{λ}^+ and δz_{λ}^- to become correlated. To model how this correlation affects $\langle \epsilon_{\lambda}^+ \rangle$, we assume that $\langle \epsilon_{\lambda}^+ \rangle$ is dominated by δz_{λ}^+ fluctuations in the tail of the distribution, which fill some volume Ω . We further assume that, in and around volume Ω , the z^- fluctuations at scales somewhat larger than λ are ordinary, with amplitudes comparable to the median value (2.7) for their scale. These larger-scale fluctuations provide the z^- energy that is fed into fluctuations of scale λ within volume Ω , and we make the simplifying approximation that δz_{λ}^- is driven or injected at the same rate throughout volume Ω . We also assume that nonlinear interactions at scale λ in effect damp δz_{λ}^- on the time scale $\lambda/\delta z_{\lambda}^+$, causing δz_{λ}^- to be $\propto 1/\delta z_{\lambda}^+$ in volume Ω . Choosing the proportionality factor so that $\delta z_{\lambda}^- \rightarrow w_{\lambda}^-$ as $\delta z_{\lambda}^+ \rightarrow w_{\lambda}^+$, we find that

$$\delta z_{\lambda}^- \sim \frac{w_{\lambda}^- w_{\lambda}^+}{\delta z_{\lambda}^+} \quad (2.20)$$

in volume Ω , which corresponds to the tail of the δz_{λ}^+ distribution. (Our estimate of δz_{λ}^- in (2.20) differs from the estimate of δz_{λ}^- in CSM15 for reasons that we discuss in § 4.)

Upon substituting (2.20) into (2.19), averaging, and making use of (2.7), (2.9) and (2.10), we obtain

$$\langle \epsilon_{\lambda}^+ \rangle \sim \frac{\langle \delta z_{\lambda}^+ \rangle w_{\lambda}^+ w_{\lambda}^-}{\lambda} \propto \lambda^{-\beta-2 \ln \beta}. \quad (2.21)$$

Equation (2.18) then implies that

$$\beta = -2 \ln \beta. \quad (2.22)$$

The solution to (2.22) is

$$\beta = 2W_0(1/2) = 0.7035, \quad (2.23)$$

where W_0 is the Lambert W function. We note that the δz_{λ}^+ fluctuations that make the largest contribution to $\langle \epsilon_{\lambda}^+ \rangle$ in (2.21) have amplitudes $\simeq \delta z_{(1),\lambda}^+ \propto \lambda^{-\beta \ln \beta} = \lambda^{0.247}$, where $\delta z_{(1),\lambda}^+$ is defined in (2.11). Deep in the inertial range, $\delta z_{(1),\lambda}^+ \gg w_{\lambda}^+ \propto \lambda^{-\ln \beta} = \lambda^{0.352}$, consistent with our assumption that $\langle \epsilon_{\lambda}^+ \rangle$ is dominated by the tail of the δz_{λ}^+ distribution.

One might expect that, in reflection-driven MHD turbulence, the spatial distribution of δz_{λ}^- should mirror the spatial distribution of δz_{λ}^+ , so that δz_{λ}^+ and δz_{λ}^- are highly correlated. However, the reflection of inertial-range z^+ fluctuations produces inertial-range z^- fluctuations with a very steep spectrum (Velli *et al.* 1989). As a consequence, the inertial-range δz_{λ}^- fluctuations are primarily the result of z^- energy that originates from the reflection of outer-scale z^+ fluctuations and that subsequently cascades to smaller scales. We do not expect the spatial distribution

of such ‘cascaded’ δz_λ^- fluctuations to approximate the spatial distribution of δz_λ^+ fluctuations in the inertial range, and indeed we have argued in (2.20) that δz_λ^+ and δz_λ^- are anticorrelated.

From (2.11), the fluctuations that make the largest contribution to the second-order structure function have amplitude

$$\delta z_{(2),\lambda}^\pm \propto \lambda^{-\beta^2 \ln \beta} = \lambda^{0.174}, \quad (2.24)$$

whereas the root-mean-square fluctuation amplitude scales as

$$\delta z_{(\text{rms}),\lambda}^\pm \equiv \left\langle (\delta z_\lambda^\pm)^2 \right\rangle^{1/2} \propto \lambda^{(1-\beta^2)/2} = \lambda^{0.253}. \quad (2.25)$$

The scaling in (2.24) is shallower than in (2.25) because the second-order structure function is dominated by a fraction f_λ of the volume that decreases as λ decreases, within which the z^\pm fluctuations are unusually strong. This volume filling factor f_λ could be defined in different ways, one being the relation $[\delta z_{(\text{rms}),\lambda}^\pm]^2 \sim f_\lambda [\delta z_{(2),\lambda}^\pm]^2$. The parallel length scale l_λ that can be inferred from an analysis of the second-order z^+ structure function (see, e.g. Sioulas *et al.* 2024) is approximately the value of l_λ within the fraction f_λ of the volume that makes the dominant contribution to $\langle (\delta z_\lambda^+)^2 \rangle$, which is approximately

$$l_{(2),\lambda} \equiv \frac{v_A \lambda}{\delta z_{(2),\lambda}^+} \propto \lambda^{1+\beta^2 \ln \beta} = \lambda^{0.826}. \quad (2.26)$$

To connect our results to the Elsasser power spectra, we take $E^\pm(f)$ to be the z^\pm power spectrum measured by a spacecraft in the solar wind, where f is frequency in the spacecraft frame. Setting $f \sim U/\lambda$, where U is the plasma velocity in the spacecraft frame, and taking $fE^\pm(f)$ to be $\propto \langle (\delta z_\lambda^\pm)^2 \rangle$, we obtain

$$E^\pm(f) \propto f^{-1-\zeta_2} = f^{-1.51}. \quad (2.27)$$

3. Comparison with observations

We compare our model with the analysis by Sioulas *et al.* (2024) of magnetic-field fluctuations during the first perihelion encounter (E1) of the Parker Solar Probe (PSP), from 1 November, 2018, to 11 November, 2018, when PSP’s heliocentric distance r ranged between 0.166 and 0.244 astronomical units (au). Sioulas *et al.* (2024) analyzed the merged SCAm data product (Bowen *et al.* 2020), which combines measurements from the flux-gate magnetometers and search-coil magnetometer of the PSP FIELDS instrument suite (Bale *et al.* 2016). Sioulas *et al.* (2024) subdivided the data into 12 hr intervals, with 6 hrs of overlap between consecutive intervals, and restricted their analysis to intervals in which the absolute value of the fractional cross-helicity

$$\sigma_c = \frac{\langle (\delta z_\lambda^+)^2 - (\delta z_\lambda^-)^2 \rangle}{\langle (\delta z_\lambda^+)^2 + (\delta z_\lambda^-)^2 \rangle} \quad (3.1)$$

exceeded 0.75 at $\lambda = 10^4 d_i$, where d_i is the proton inertial length. Sioulas *et al.* (2024) then computed five-point structure functions of the magnetic field in a coordinate system in which one axis (the l axis) is aligned with the local background

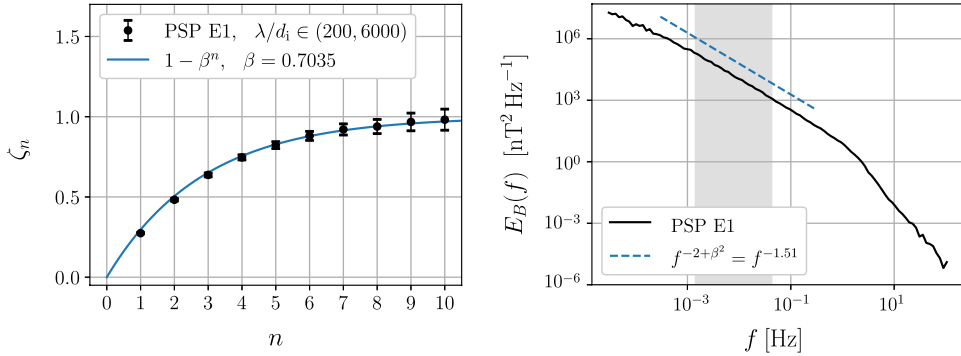


FIGURE 1. (a) The scaling exponent ζ_n of the n th-order \mathbf{z}^+ structure function from (2.10) and (2.23), and the scaling exponent of the n th-order magnetic-field structure function obtained by Sioulas *et al.* (2024) from measurements during PSP’s first perihelion encounter. (b) The power spectrum $E_B(f)$ of the magnetic field in PSP encounter-1 data as a function of spacecraft-frame frequency f , as well as the \mathbf{z}^+ power-spectrum scaling from (2.27). The shaded grey rectangle shows the frequency interval that corresponds to the scale range $200d_i < \lambda < 6000d_i$ based on the correspondence $f = U/(2\lambda)$ suggested by figure 1 of Huang *et al.* (2023), with $U = 277 \text{ km s}^{-1}$ and $d_i = 16.3 \text{ km}$.

magnetic field $\mathbf{B}_{\text{local}}$, a second axis (the ξ axis) is aligned with the component of the magnetic-field fluctuation perpendicular to $\mathbf{B}_{\text{local}}$, and the third axis (the λ axis) is perpendicular to the first two. Each increment $\Delta\mathbf{B}$ computed from the data corresponds to a spatial separation $\Delta\mathbf{x}$ parallel to the instantaneous value of the relative velocity between the plasma and spacecraft, which in general has a non-zero component along each of the l , ξ and λ directions. Sioulas *et al.* (2024) considered three different subsets of increments, one in which $\Delta\mathbf{x}$ is within 5° of the l direction, one in which $\Delta\mathbf{x}$ is within 5° of the ξ direction and one in which $\Delta\mathbf{x}$ is within 5° of the λ direction. It is this last subset that we compare with our model results in this section.

To convert time intervals into spatial intervals, Sioulas *et al.* (2024) applied Taylor’s frozen-flow hypothesis based on the average plasma velocity U in the spacecraft frame. Plasma measurements from the SWEAP instrument suite (Kasper *et al.* 2016) show that the average value of U during the selected intervals was 277 km s^{-1} . Quasithermal-noise electron-density measurements from FIELDS data (Moncuquet *et al.* 2020) and quasineutrality imply that the average value of d_i during the selected intervals was 16.3 km .

Within the large- σ_c intervals analysed by Sioulas *et al.* (2024), $\delta z_\lambda^- \ll \delta z_\lambda^+$, and hence $\delta z_\lambda^+ \simeq 2\delta B_\lambda / \sqrt{4\pi\rho}$, where δB_λ is defined by analogy to (2.2). We thus expect the structure functions of \mathbf{B} in these intervals to scale with λ in the same way as the \mathbf{z}^+ structures functions. In figure 1(a), we plot the magnetic-field structure-function scaling exponents obtained by Sioulas *et al.* (2024) over the range $200d_i < \lambda < 6000d_i$, as well as the \mathbf{z}^+ structure-function scaling exponents from (2.10) and (2.23). The error bars on the scaling exponents are the errors associated with the power-law fits to the structure functions and do not account for errors arising from the sensitivity of high-order structure functions to rare events in the tail of the distribution (see, e.g. Dudok de Wit *et al.* 2013). Further work is needed to quantify such errors; here we simply note that the observationally inferred ζ_n values at large n in figure 1 should be viewed with caution.

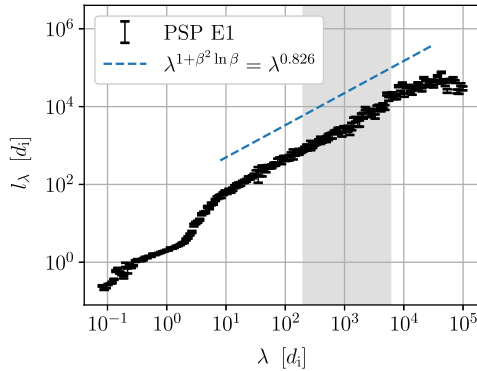


FIGURE 2. The parallel correlation length l_λ inferred from PSP magnetic-field measurements (Sioulas *et al.* 2024), and the $l_{(2),\lambda}$ scaling from (2.26). The shaded rectangle corresponds to the scale range that was used to calculate the PSP E1 structure-function scaling exponents in figure 1.

Using the subset of E1 magnetic-field increments obtained by Sioulas *et al.* (2024) in which $\Delta \mathbf{x}$ is within 5° of the λ direction, we compute the conditional power spectral density of the magnetic field, $E_B(f)$, obtained via the maximum overlap discrete wavelet transform (Percival & Walden 2000), where f is frequency in the spacecraft frame. We plot $E_B(f)$ in figure 1(b), as well as the Elsasser power-spectrum scaling from (2.27).

In figure 2 we plot the result of Sioulas *et al.* (2024) for the scale-dependent parallel correlation length l_λ , which they obtained by comparing the parallel second-order structure function $SF_{2\parallel}(l)$ in which $\Delta \mathbf{x}$ is within 5° of the l direction and the perpendicular second-order structure function $SF_{2\perp}(\lambda)$ obtained from increments in which $\Delta \mathbf{x}$ is within 5° of the λ direction. They defined l_λ to be that value of l for which $SF_{2\perp}(\lambda) = SF_{2\parallel}(l)$. We also plot in figure 2 the scaling $l_{(2),\lambda} \propto \lambda^{1+\beta^2 \ln \beta} = \lambda^{0.826}$ from (2.26) for the fluctuations that make the largest contribution to the second-order structure function of \mathbf{z}^+ .

Our model agrees quite well with the power spectrum and ζ_n values inferred by Sioulas *et al.* (2024) from PSP E1 data for the scale range $200d_i < \lambda < 6000d_i$. We note, however, that the ζ_n values that Sioulas *et al.* (2024) found for the scale range $8d_i < \lambda < 100d_i$ are larger than those shown in figure 1 and do not agree with our model. On the other hand, the scaling of $l_{(2),\lambda}$ in (2.26) agrees reasonably well with the l_λ values inferred by Sioulas *et al.* (2024) over the broader scale range $8d_i < \lambda < 3 \times 10^4 d_i$.

4. Comparison with models of balanced, intermittent, homogeneous RMHD turbulence

Our model shares several features with the previous models of CSM15 and MS17, which were developed for balanced (i.e. zero-cross-helicity), intermittent, homogeneous RMHD turbulence. In particular, we adopt the same procedure in (2.3) and (2.4) for determining the scale dependence of the fluctuation-amplitude distribution and the same volume filling factor in (2.4) and (2.6) for the most intense δz_λ^+ fluctuations. As a consequence, we obtain the same formula, (2.10), as these previous authors for the scaling exponent ζ_n of the n th-order structure function of δz_λ^+ .

These shared assumptions receive considerable support from the results of Sioulas *et al.* (2024) on the structure-function scaling exponents of magnetic fluctuations in the scale range $200d_i < \lambda < 6000d_i$ in the near-Sun solar wind, which are shown in figure 1. In particular, the finding of Sioulas *et al.* (2024) that ζ_n asymptotes to a constant value at large n implies that the amplitude of the most intense fluctuations at scale λ is independent of λ , consistent with (2.3). Moreover, the finding of Sioulas *et al.* (2024) that ζ_n asymptotes to $\simeq 1$ at large n implies that the volume filling factor of the most intense fluctuations is $\propto \lambda$, consistent with (2.4) and (2.6).

On the other hand, we depart from CSM15 and MS17 by taking large-amplitude fluctuations to be tube-like. In contrast, CSM15 and MS17 took such fluctuations to be sheet-like, in agreement with numerical simulations of homogeneous MHD turbulence (e.g. Maron & Goldreich 2001). Our assumption of tube-like fluctuations is motivated by the results of Sioulas *et al.* (2024) on the three-dimensional geometry of the second-order structure function of the magnetic field in the scale range $200d_i < \lambda < 6000d_i$ in PSP data.

The assumption of CSM15 that fluctuations in the tail of the distribution are sheet-like led them to the conclusion that l_λ^+ is an increasing function of δz_λ^+ . To explain this, we briefly review CSM15's analysis of the interaction between large-amplitude, sheet-like \mathbf{z}^+ structures and much weaker, counter-propagating \mathbf{z}^- fluctuations. CSM15 characterized sheet-like \mathbf{z}^+ structures in the tail of the distribution as having dimensions l_λ^+ in the \mathbf{B} direction, ξ_λ in the $\Delta\mathbf{z}_\lambda^+$ direction, and λ in the $\mathbf{B} \times \Delta\mathbf{z}_\lambda^+$ direction, with $\xi_\lambda \gg \lambda$ and $\xi_\lambda \propto \delta z_\lambda^\pm$. To determine the rate of deformation of a sheet-like δz_λ^+ structure, CSM15 defined a trial-volume sphere of radius $\sim \lambda$ located somewhere in the middle of the sheet. Noting that the \mathbf{z}^- fluctuations propagating at velocity v_A within that trial volume have been preprocessed by the part of the \mathbf{z}^+ sheet upstream of the trial volume, CSM15 defined the 'source region' for the \mathbf{z}^- fluctuations in the trial volume to be the region upstream of the trial volume closest to the trial volume within which the \mathbf{z}^- fluctuations have not yet interacted with the \mathbf{z}^+ sheet. CSM15 made the approximation that the \mathbf{z}^- fluctuations in this source region are median-amplitude \mathbf{z}^- fluctuations, which are tube-like in the CSM15 model. CSM15 used the notation l_λ^* to denote the parallel correlation length of such median-amplitude fluctuations at perpendicular scale λ . CSM15 then showed that the \mathbf{z}^- fluctuations in the trial volume that are most effective at shearing the \mathbf{z}^+ structure are the \mathbf{z}^- fluctuations that had a perpendicular scale ξ_λ in the source region. As these \mathbf{z}^- fluctuations propagate from the source region to the trial volume, shearing by the \mathbf{z}^+ sheet reduces their correlation length in the $\mathbf{B} \times \Delta\mathbf{z}_\lambda^+$ direction from ξ_λ to λ and rotates them into alignment with the \mathbf{z}^+ sheet, so that the angle θ_λ^\pm between $\Delta\mathbf{z}_\lambda^+$ and $\Delta\mathbf{z}_\lambda^-$ within the trial volume is small, which decreases the rate at which the \mathbf{z}^- fluctuations shear the \mathbf{z}^+ structure.

CSM15 estimated l_λ^+ using two different arguments. First, CSM15 set $l_\lambda^+ \sim v_A \tau_\lambda^+$, taking the parallel correlation length of a \mathbf{z}^+ fluctuation to be the distance it can propagate along the magnetic field before its energy cascades to smaller scales. We call this the survival-time argument. Second, CSM15 took l_λ^+ for a \mathbf{z}^+ structure to be the parallel correlation length of the \mathbf{z}^- fluctuations that dominate the shearing of the \mathbf{z}^+ structure and evaluating the parallel correlation length of those \mathbf{z}^- fluctuations before they started interacting with the \mathbf{z}^+ structure – i.e. in the source region described in the previous paragraph. This led to the estimate $l_\lambda^+ \sim l_{\xi_\lambda}^*$. We call this second argument the agent-of-shearing argument. CSM15 showed that these two arguments lead to the same estimate for l_λ^+ , i.e. that $v_A \tau_\lambda^+ \sim l_{\xi_\lambda}^*$.

These two arguments were the basis for CSM15's aforementioned conclusion that l_λ^+ is an increasing function of δz_λ^+ . For the agent-of-shearing argument, this is because ξ_λ is an increasing function of δz_λ^+ , and hence so is $l_{\xi_\lambda}^*$. For the survival-time argument, this is because as δz_λ^+ increases, θ_λ^\pm decreases, the cascade time scale τ_λ^+ increases, and the z^+ fluctuation propagates farther before cascading.⁴

In our model, large-amplitude fluctuations are tube-like and therefore their nonlinear interactions are not described by the analysis of CSM15. In particular, there is no preprocessing of z^- fluctuations as they propagate from a preinteraction source region through an extended sheet-like z^+ structure, and nonlinear interactions do not cause z^+ and z^- fluctuations to become progressively more aligned as δz_λ^+ increases. We estimate $l_\lambda^- \sim v_A \lambda / \delta z_\lambda^+$ in (2.13) using the survival-time argument. We then use the agent-of-shearing argument to estimate l_λ^+ in (2.14), setting $l_\lambda^+ \sim l_\lambda^-$. This latter estimate makes our survival-time estimate of l_λ^- consistent with the agent-of-shearing estimate of l_λ^- . However, our agent-of-shearing estimate of l_λ^+ differs from the survival-time estimate of l_λ^+ , because $v_A \tau_\lambda^+ \sim v_A \lambda / \delta z_\lambda^- \gg l_\lambda^- \sim v_A \lambda / \delta z_\lambda^+$. Thus, although CSM15 did not need to choose between the agent-of-shearing argument and the survival-time argument to determine l_λ^+ , we do need to choose, and we choose the agent-of-shearing argument.

Whereas CSM15 found that l_λ^+ is an increasing function of δz_λ^+ in balanced RMHD turbulence, we find in (2.13) and (2.14) that l_λ^+ is a decreasing function of δz_λ^+ in imbalanced, reflection-driven, Alfvénic turbulence. Because δz_λ^+ exceeds $\delta z_{\text{rms},\lambda}^+$ within the small fraction of the volume that dominates the second-order z^+ structure function (see (2.24) and (2.25)), l_λ^+ is smaller in this small fraction of the volume than it would be throughout the plasma as a whole in a turbulence model that neglects intermittency. Intermittency in reflection-driven Alfvénic turbulence thus increases the effective parallel wavenumbers $k_\parallel \sim 1/l_\lambda^+$ of the energetically dominant fluctuations at small λ , making these fluctuations more isotropic.

Our assumption that large-amplitude z^+ fluctuations are tube-like also explains why our estimate of δz_λ^- in (2.20) differs from the estimate of CSM15. CSM15 showed that when a large-amplitude, sheet-like z^+ structure interacts with a smaller-amplitude z^- fluctuation, the amplitude of the z^- fluctuation is not altered. In contrast, in our analysis, large-amplitude, tube-like z^+ fluctuations can alter, and in particular decrease, the amplitudes of the z^- fluctuations with which they interact.

4.1. The volume filling factor and geometry of the most intense fluctuations

As mentioned in §2 and at the beginning of §4, we follow previous studies by assuming in (2.6) that the volume filling factor of the most intense fluctuations is $\propto \lambda$ (Grauer *et al.* 1994; Politano & Pouquet 1995; Chandran *et al.* 2015; Mallet & Schekochihin 2017). The usual justification for this assumption is to posit that the most intense fluctuations at all λ are associated with the same set of sheet-like discontinuities. If the two locations $\mathbf{x} \pm 0.5\lambda\hat{\mathbf{s}}$ that determine the Elsasser increment

⁴We note that the dominant nonlinear interactions in the CSM15 model exhibit three different types of locality. Within the trial volume, the dominant nonlinear interactions are between z^+ and z^- fluctuations with the same perpendicular scale λ . When the dimensions of a sheet-like z^+ fluctuation are compared with the dimensions of the tube-like, median-amplitude z^- fluctuations of perpendicular scale ξ_λ in the source region, the perpendicular correlation length of these z^- fluctuations matches the width ξ_λ of the z^+ sheet, not the thickness λ of the sheet, and the parallel correlation length of the z^- fluctuations matches the parallel correlation length of the z^+ sheet.

$\Delta z_\lambda^\pm(\mathbf{x}, \hat{\mathbf{s}}, t)$ in (2.1) are regarded as a two-point probe, then the probability that this two-point probe straddles (and therefore detects) one of these sheet-like discontinuities within some volume V of turbulent plasma is $\sim A\lambda/V$, where A is the combined area of the sheet-like discontinuities within that volume.

This line of reasoning is self-consistent within the CMS15 and MS17 models, which take the large-amplitude fluctuations in the tail of the distribution to be sheet-like. It becomes problematic, however, in our model, because we have taken the large-amplitude fluctuations that dominate the energy cascade to be tube-like, as suggested by the findings of Sioulas *et al.* (2024) regarding the three-dimensional geometry of the second-order structure function of the magnetic field in the near-Sun solar wind at $200d_i < \lambda < 6000d_i$. The observed dominance of tube-like fluctuations in this scale range might appear to suggest that we should adopt a different scaling for the volume filling factor of the largest-amplitude fluctuations. However, the observations reported by Sioulas *et al.* (2024) suggest that $\zeta_n \rightarrow 1$ as $n \rightarrow \infty$ within this same range of scales, an asymptotic behaviour that directly implies that the filling factor of the most intense fluctuations is $\propto \lambda$, as discussed at the beginning of §4.

To summarize the previous two paragraphs, the observation that $\zeta_n \rightarrow 1$ at large n suggests that large-amplitude fluctuations are sheet-like, but the measured second-order structure function suggests that large-amplitude fluctuations are tube-like. One possible way to resolve this tension relates to the fact the second-order structure function is dominated by fluctuations in the near tail of the probability distribution function (PDF) with amplitudes $\simeq \delta z_{(2),\lambda}^+$, whereas the filling-factor assumption embedded in (2.6) describes fluctuations in the extreme tail of the PDF with amplitudes $\simeq \bar{z}^+$. These two different parts of the PDF could arise from different physical processes. For example, fluctuations in the near tail could be tube-like because of the (as yet not fully understood) dynamics of the nonlinear interactions that give rise to the energy cascade in reflection-driven Alfvénic turbulence, while fluctuations in the extreme tail of the PDF could result from switchbacks – sheet-like discontinuities in \mathbf{z}^+ that pervade the near-Sun solar wind (Kasper *et al.* 2019; Bale *et al.* 2019; Horbury *et al.* 2020). Switchbacks are likely produced by the tendency of imbalanced MHD turbulence in compressible plasmas to evolve towards a state of spherical polarization (e.g. Squire, Chandran & Meyrand 2020; Shoda, Chandran & Cranmer 2021; Mallet *et al.* 2021). In this picture, the energy cascade (see (2.21) and the discussion following (2.23)) and second-order δz_λ^+ structure function are dominated by tube-like fluctuations in the near tail of the PDF, but the value of ζ_n at large n is controlled by sheet-like switchbacks. Further work, however, is needed to determine whether such a hybrid picture of the PDF is relevant to the solar wind.

5. Conclusion

In this paper, we have drawn upon several elements of the Lithwick *et al.* (2007) theory of strong, imbalanced MHD turbulence to develop a phenomenological model of intermittent, reflection-driven Alfvénic turbulence. Our treatment of intermittency is based upon three principal conjectures. First, we adopt a particular mathematical model, given by (2.3) and (2.4), for determining the scale dependence of the PDF of fluctuation amplitudes – the same model that was adopted by CSM15 and MS17. Second, we assume the same scaling as these authors for the volume filling factor of the most intense fluctuations at each scale. Third, we conjecture in (2.20) that, within the small fraction of the volume that dominates $\langle \epsilon_\lambda^+ \rangle$ in which δz_λ^+ is unusually strong, δz_λ^- becomes anticorrelated with δz_λ^+ because of the strong

shearing experienced by δz^- fluctuations where δz_λ^+ is large. This third conjecture departs from the analysis of CSM15, a contrast that results ultimately from our differing assumptions about the geometry of the fluctuations in the near tail of the distribution that dominate $\langle \epsilon_\lambda^+ \rangle$ (see § 4). Although our model relies on these conjectures, it contains no adjustable fitting parameters. Our model predicts the scaling of the inertial-range power spectrum, the structure-function scaling exponent ζ_n of the n th-order structure function for all n , and the scaling of l_λ^\pm with λ . These predictions agree reasonably well with the corresponding scalings inferred by Sioulas *et al.* (2024) from PSP data at $200d_i < \lambda < 6000d_i$.

Our findings, and the PSP observations with which they agree, have important implications for the dissipation of reflection-driven turbulence at small scales. As in previous models of intermittency in MHD turbulence, we find that the small-scale structures that control the turbulent heating rate have larger amplitudes than in turbulence theories that neglect intermittency. These enhanced amplitudes increase the rate of stochastic ion heating, as noted in previous studies (e.g. Chandran *et al.* 2010; Xia *et al.* 2013; Mallet *et al.* 2019). Whereas CSM15 found that intermittency increases l_λ at small λ within the intense fluctuations that dominate the energy in balanced homogeneous MHD turbulence, we find that intermittency in reflection-driven Alfvénic turbulence has the opposite effect, making the fluctuations that dominate the energy at small λ more isotropic. This acts to increase the frequencies of these small-scale fluctuations, possibly to the point that they can trigger significant ion cyclotron heating, at least in some regions of the solar corona and solar wind.

Important directions for future research include clarifying and explaining the amplitude distribution and three-dimensional anisotropy of fluctuations in the solar wind and in numerical simulations of reflection-driven Alfvénic turbulence and determining the reasons for the differences between the turbulence scalings seen in PSP data at $200d_i < \lambda < 6000d_i$ and $8d_i < \lambda < 100d_i$ (Sioulas *et al.* 2024). Other useful directions for future research include using direct numerical simulations and a wider variety of observational data to test our results and modelling assumptions and exploring the consequences of our model for ion cyclotron heating in the solar corona and solar wind.

Acknowledgements

B.C. thanks A. Mallet and A. Schekochihin for many valuable discussions of intermittency in MHD turbulence and J. Hollweg, J. Perez, J. Squire and M. Velli for helpful discussions of reflection-driven turbulence. The authors thank the anonymous reviewers for helpful comments and criticisms that led to improvements in the manuscript.

Editor Alex Schekochihin thanks the referees for their advice in evaluating this article.

Funding

This work was supported in part by NASA grant NNN06AA01C to the Parker Solar Probe FIELDS Experiment and by NASA grants 80NSSC24K0171 and 80NSSC21K1768.

Declaration of interests

The authors report no conflict of interest.

REFERENCES

- BALE, S.D., et al. 2019 Highly structured slow solar wind emerging from an equatorial coronal hole. *Nature* **576** (7786), 237–242.
- BALE, S.D. et al. 2016 The FIELDs instrument suite for solar probe plus. Measuring the coronal plasma and magnetic field, plasma waves and turbulence, and radio signatures of solar transients. *Space Sci. Rev.* **204** (1–4), 49–82.
- BERESNYAK, A. & LAZARIAN, A. 2008 Strong imbalanced turbulence. *Astrophys. J.* **682** (2), 1070–1075.
- BOWEN, T.A., et al. 2020 A merged search-coil and fluxgate magnetometer data product for Parker Solar Probe FIELDs. *J. Geophys. Res. (Space Phys.)* **125** (5), e27813.
- CHANDRAN, B.D.G. 2008 Strong anisotropic MHD turbulence with cross helicity. *Astrophys. J.* **685** (1), 646–658.
- CHANDRAN, B.D.G., LI, B., ROGERS, B.N., QUATAERT, E. & GERMASCHEWSKI, K. 2010 Perpendicular ion heating by low-frequency Alfvén-wave turbulence in the solar wind. *Astrophys. J.* **720** (1), 503–515.
- CHANDRAN, B.D.G. & PEREZ, J.C. 2019 Reflection-driven magnetohydrodynamic turbulence in the solar atmosphere and solar wind. *J. Plasma Phys.* **85** (4), 905850409.
- CHANDRAN, B.D.G., SCHEKOCHIHIN, A.A. & MALLET, A. 2015 Intermittency and alignment in strong RMHD turbulence. *Astrophys. J.* **807** (1), 39.
- CHO, J. & VISHNIAC, E.T. 2000 The anisotropy of magnetohydrodynamic Alfvénic turbulence. *Astrophys. J.* **539** (1), 273–282.
- CHOI, K.P. 1994 On the medians of gamma distributions and an equation of Ramanujan. *Proc. Am. Math. Soc.* **62** (1), 242–251.
- DMITRUK, P. & MATTHAEUS, W.H. 2003 Low-frequency waves and turbulence in an open magnetic region: timescales and heating efficiency. *Astrophys. J.* **597** (2), 1097–1105.
- DUDOK DE WIT, T., ALEXANDROVA, O., FURNO, I., SORRISO-VALVO, L. & ZIMBARDO, G. 2013 Methods for characterising microphysical processes in plasmas. *Space Sci. Rev.* **178** (2–4), 665–693.
- ELSASSER, W.M. 1950 The hydromagnetic equations. *Phys. Rev.* **79** (1), 183–183.
- FRISCH, U. 1996 *Turbulence*. Cambridge University Press.
- GALTIER, S., NAZARENKO, S.V., NEWELL, A.C. & POUQUET, A. 2000 A weak turbulence theory for incompressible magnetohydrodynamics. *J. Plasma Phys.* **63** (5), 447–488.
- GOLDREICH, P. & SRIDHAR, S. 1995 Toward a theory of interstellar turbulence. 2: strong Alfvénic turbulence. *Astrophys. J.* **438**, 763–775.
- GRAUER, R., KRUG, J. & MARLIANI, C. 1994 Scaling of high-order structure functions in magnetohydrodynamic turbulence. *Phys. Lett. A* **195** (5–6), 335–338.
- HEINEMANN, M. & OLBERT, S. 1980 Non-WKB Alfvén waves in the solar wind. *J. Geophys. Res.* **85** (A3), 1311–1327.
- HOLLWEG, J.V. & ISENBERG, P.A. 2007 Reflection of Alfvén waves in the corona and solar wind: an impulse function approach. *J. Geophys. Res. (Space Phys.)* **112**, 8102.
- HORBURY, T.S., et al. 2020 Sharp Alfvénic impulses in the near-sun solar wind. *Astrophys. J.* **246** (2), 45.
- HUANG, Z., et al. 2023 New observations of solar wind 1/f turbulence spectrum from Parker Solar Probe. *Astrophys. J. Lett.* **950** (1), L8.
- KADOMTSEV, B.B. & POGUTSE, O.P. 1974 Nonlinear helical perturbations of a plasma in the tokamak. *Sov. J. Exp. Theor. Phys.* **38**, 283.
- KASPER, J.C., et al. 2016 Solar wind electrons alphas and protons (SWEAP) investigation: design of the solar wind and coronal plasma instrument suite for solar probe plus. *Space Sci. Rev.* **204** (1–4), 131–186.
- KASPER, J.C., et al. 2019 Alfvénic velocity spikes and rotational flows in the near-sun solar wind. *Nature* **576** (7786), 228–231.

- KRAICHNAN, R.H. 1965 Inertial-range spectrum of hydromagnetic turbulence. *Phys. Fluids* **8** (7), 1385–1387.
- LITHWICK, Y., GOLDBREICH, P. & SRIDHAR, S. 2007 Imbalanced strong MHD turbulence. *Astrophys. J.* **655** (1), 269–274.
- MALLET, A., KLEIN, K.G., CHANDRAN, B.D.G., GROŠELJ, D. & HOPPOCK, I.W. 2019 Interplay between intermittency and dissipation in collisionless plasma turbulence. *J. Plasma Phys.* **85** (3), 175850302.
- MALLET, A. & SCHEKOCHIHIN, A.A. 2017 A statistical model of three-dimensional anisotropy and intermittency in strong Alfvénic turbulence. *Mon. Not. R. Astron. Soc.* **466** (4), 3918–3927.
- MALLET, A., SCHEKOCHIHIN, A.A. & CHANDRAN, B.D.G. 2015 Refined critical balance in strong Alfvénic turbulence. *Mon. Not. R. Astron. Soc.* **449** (1), L77–L81.
- MALLET, A., SQUIRE, J., CHANDRAN, B.D.G., BOWEN, T. & BALE, S.D. 2021 Evolution of large-amplitude Alfvén waves and generation of switchbacks in the expanding solar wind. *Astrophys. J.* **918** (2), 62.
- MARON, J. & GOLDBREICH, P. 2001 Simulations of incompressible magnetohydrodynamic turbulence. *Astrophys. J.* **554** (2), 1175–1196.
- MATTHAEUS, W.H., ZANK, G.P., OUGHTON, S., MULLAN, D.J. & DMITRUK, P. 1999 Coronal heating by magnetohydrodynamic turbulence driven by reflected low-frequency waves. *Astrophys. J. Lett.* **523** (1), L93–L96.
- MEYRAND, R., SQUIRE, J., MALLET, A. & CHANDRAN, B.D.G. 2025 Reflection-driven turbulence in the super-Alfvénic solar wind. *J. Plasma Phys.* **91** (1), E29.
- MONCUQUET, M., et al. 2020 First in situ measurements of electron density and temperature from quasi-thermal noise spectroscopy with Parker Solar Probe/FIELDS. *Astrophys. J.* **246** (2), 44.
- MONTGOMERY, D. & TURNER, L. 1981 Anisotropic magnetohydrodynamic turbulence in a strong external magnetic field. *Phys. Fluids*, **24**, 825.
- NG, C.S. & BHATTACHARJEE, A. 1996 Interaction of shear-alfven wave packets: implication for weak magnetohydrodynamic turbulence in astrophysical plasmas. *Astrophys. J.* **465**, 845.
- NG, C.S. & BHATTACHARJEE, A. 1997 Scaling of anisotropic spectra due to the weak interaction of shear-Alfvén wave packets. *Phys. Plasmas* **4** (3), 605–610.
- PERCIVAL, D. & WALDEN, A. 2000 *Wavelet Methods for Time Series Analysis*. Cambridge University Press.
- PEREZ, J.C. & BOLDYREV, S. 2009 Role of cross-helicity in magnetohydrodynamic turbulence. *Phys. Rev. Lett.* **102** (2), 025003.
- PEREZ, J.C. & CHANDRAN, B.D.G. 2013 Direct numerical simulations of reflection-driven, reduced MHD turbulence from the sun to the Alfvén critical point. *Astrophys. J.* **776** (2), 124.
- PODESTA, J.J. & BHATTACHARJEE, A. 2010 Theory of incompressible magnetohydrodynamic turbulence with scale-dependent alignment and cross-helicity. *Astrophys. J.* **718** (2), 1151–1157.
- POLITANO, H. & POUQUET, A. 1995 Model of intermittency in magnetohydrodynamic turbulence. *Phys. Rev. E* **52** (1), 636–641.
- SCHEKOCHIHIN, A.A. 2022 MHD turbulence: a biased review. *J. Plasma Phys.* **88** (5), 155880501.
- SCHEKOCHIHIN, A.A., COWLEY, S.C., DORLAND, W., HAMMETT, G.W., HOWES, G.G., QUATAERT, E. & TATSUNO, T. 2009 Astrophysical gyrokinetics: kinetic and fluid turbulent cascades in magnetized weakly collisional plasmas. *Astrophys. J. Suppl.* **182**, 310–377.
- SHE, Z.-S. & LEVEQUE, E. 1994 Universal scaling laws in fully developed turbulence. *Phys. Rev. Lett.* **72** (3), 336–339.
- SHEBALIN, J.V., MATTHAEUS, W. & MONTGOMERY, D. 1983 Anisotropy in MHD turbulence due to a mean magnetic field. *J. Plasma Phys.* **29** (3), 525–547.
- SHODA, M., CHANDRAN, B.D.G. & CRANMER, S.R. 2021 Turbulent generation of magnetic switchbacks in the Alfvénic solar wind. *Astrophys. J.* **915** (1), 52.
- SIOULAS, N., et al. 2024 Higher-order analysis of three-dimensional anisotropy in imbalanced Alfvénic turbulence. arXiv e-prints p. arXiv: 2404.04055.
- SQUIRE, J., CHANDRAN, B.D.G. & MEYRAND, R. 2020 In-situ switchback formation in the expanding solar wind. *Astrophys. J. Lett.* **891** (1), L2.

- STRAUSS, H.R. 1976 Nonlinear, three-dimensional magnetohydrodynamics of noncircular tokamaks. *Phys. Fluids* **19** (1), 134–140.
- TU, C. & MARSCH, E. 1995 MHD structures, waves and turbulence in the solar wind: observations and theories. *Space Sci. Rev.* **73** (1-2), 1–210.
- VAN BALLEGOIJEN, A.A. & ASGARI-TARGHI, M. 2016 Heating and acceleration of the fast solar wind by Alfvén wave turbulence. *Astrophys. J.* **821** (2), 106.
- VAN BALLEGOIJEN, A.A. & ASGARI-TARGHI, M. 2017 Direct and inverse cascades in the acceleration region of the fast solar wind. *Astrophys. J.* **835** (1), 10.
- VAN BALLEGOIJEN, A.A., ASGARI-TARGHI, M., CRANMER, S.R. & DELUCA, E.E. 2011 Heating of the solar chromosphere and corona by Alfvén wave turbulence. *Astrophys. J.* **736** (1), 3.
- VELLI, M. 1993 On the propagation of ideal, linear Alfvén waves in radially stratified stellar atmospheres and winds. *Astron. Astrophys.* **270**, 304–314.
- VELLI, M., GRAPPIN, R. & MANGENEY, A. 1989 Turbulent cascade of incompressible unidirectional Alfvén waves in the interplanetary medium. *Phys. Rev. Lett.* **63** (17), 1807–1810.
- VERDINI, A. & VELLI, M. 2007 Alfvén waves and turbulence in the solar atmosphere and solar wind. *Astrophys. J.* **662** (1), 669–676.
- XIA, Q., PEREZ, J.C., CHANDRAN, B.D.G. & QUATAERT, E. 2013 Perpendicular ion heating by reduced magnetohydrodynamic turbulence. *Astrophys. J.* **776** (2), 90.